

Geophysical Research Letters

RESEARCH LETTER

10.1029/2020GL088803

Key Points:

- Comprehensive observations of the daytime Sq dynamo electrodynamics have been gathered for the first time
- Observed daytime winds in the dynamo region are much larger than expected yet their currents are reduced by those of DC electric fields
- Winds and currents exhibit an interleaved spiral pattern indicative of tidal forcing

Supporting Information:

- Supporting Information S1
- Figure S1
- Figure S2
- Figure S3
- Figure S4
- Figure S5
- Figure S6
- Figure S7
- Figure S8
- Figure S9
- Figure S10
- Figure S11
- Figure S12

Correspondence to:

R. Pfaff,
robert.f.pfaff@nasa.gov

Citation:

Pfaff, R., Larsen, M., Abe, T., Habu, H., Clemmons, J., & Freudenreich, H., et al. (2020). Daytime dynamo electrodynamics with spiral currents driven by strong winds revealed by vapor trails and sounding rocket probes. *Geophysical Research Letters*, 47, e2020GL088803. <https://doi.org/10.1029/2020GL088803>

Received 9 MAY 2020

Accepted 4 JUL 2020

Accepted article online 17 JUL 2020





















Author Contributions:

Conceptualization: R. Pfaff
Data curation: T. Bullett, J. Mabie, N. Murphy, V. Angelopoulos
(continued)

©2020. The Authors.

This is an open access article under the terms of the Creative Commons Attribution-NonCommercial-NoDerivs License, which permits use and distribution in any medium, provided the original work is properly cited, the use is non-commercial and no modifications or adaptations are made.

Daytime Dynamo Electrodynamics With Spiral Currents Driven by Strong Winds Revealed by Vapor Trails and Sounding Rocket Probes

R. Pfaff¹ , M. Larsen² , T. Abe³ , H. Habu³ , J. Clemmons⁴ , H. Freudenreich¹ , D. Rowland¹ , T. Bullett^{5,6} , M.-Y. Yamamoto⁷ , S. Watanabe⁸ , Y. Kakinami⁸ , T. Yokoyama⁹ , J. Mabie^{5,6} , J. Klenzing¹ , R. Bishop¹⁰ , R. Walterscheid¹⁰ , M. Yamamoto⁹ , Y. Yamazaki¹¹ , N. Murphy¹² , and V. Angelopoulos¹³ 

¹NASA Goddard Space Flight Center, Greenbelt, MD, USA, ²Department of Physics and Astronomy, Clemson University, Clemson, SC, USA, ³Japan Aerospace Exploration Agency, Tokyo, Japan, ⁴Department of Physics and Astronomy, University of New Hampshire, Durham, NH, USA, ⁵Cooperative Institute for Research in Environmental Sciences, University of Colorado, Boulder, CO, USA, ⁶National Oceanic and Atmospheric Administration, Boulder, CO, USA, ⁷School of Systems Engineering, Kochi University of Technology, Kami, Japan, ⁸Department of Information Media, Hokkaido Information University, Ebetsu, Japan, ⁹Research Institute for Sustainable Humanosphere, Kyoto University, Uji, Japan, ¹⁰Aerospace Corporation, El Segundo, CA, USA, ¹¹Geo Forschungs Zentrum, Potsdam, Germany, ¹²Jet Propulsion Laboratory, Pasadena, CA, USA, ¹³Department of Earth, Planetary, and Space Sciences, University of California, Los Angeles, CA, USA

Abstract We investigate the forces and atmosphere-ionosphere coupling that create atmospheric dynamo currents using two rockets launched nearly simultaneously on 4 July 2013 from Wallops Island (USA), during daytime Sq conditions with ΔH of -30 nT. One rocket released a vapor trail observed from an airplane which showed peak velocities of >160 m/s near 108 km and turbulence coincident with strong unstable shear. Electric and magnetic fields and plasma density were measured on a second rocket. The current density peaked near 110 km exhibiting a spiral pattern with altitude that mirrored that of the winds, suggesting the dynamo is driven by tidal forcing. Such stratified currents are obscured in integrated ground measurements. Large electric fields produced a current opposite to that driven by the wind, believed created to minimize the current divergence. Using the observations, we solve the dynamo equation versus altitude, providing a new perspective on the complex nature of the atmospheric dynamo.

Plain Language Summary Two rockets with scientific instruments were launched in the middle of the day to study the upper atmosphere and how it interacts with the ionosphere. The rockets ascended to altitudes of about 140 km—just high enough to gather the necessary data—before coming back down along parabolic trajectories. A vapor trail released by one rocket was photographed on an airplane and showed the upper atmosphere moving at very large speeds, much larger than previously believed. In fact, these winds were so large and changed speed so quickly that in some places the upper atmosphere became turbulent. Instruments on the second rocket gathered information about the ionosphere, including the number of ions present and how the currents and electric fields associated with those charged particles varied with altitude, particularly where the winds were strongest. The winds and currents both displayed a spiral pattern with altitude indicative that they were driven by atmospheric forcing from below. By combining all of these measurements, we are able to better determine what drives the worldwide system of currents at the base of the ionosphere. This “daytime dynamo” is a fundamental part of our natural world, swirling high above us and changing every day.

1. Introduction

Atmospheric dynamos create global systems of currents driven by winds within the conducting upper atmospheres of magnetized planets, such as Earth, Jupiter, and Saturn. The Earth's atmospheric dynamo is accessible to detailed scientific study and can be explored directly with probes on sounding rockets, revealing the interdependency of the forces that drive the dynamo and their consequential patterns of currents and electric fields.

Prior to the space age, the atmospheric dynamo, which is now known to exist at the edge of space near 100 km altitude, was studied remotely. For centuries, currents in space were inferred from magnetic

Formal analysis: T. Abe, H. Freudenreich, D. Rowland, M.-Y. Yamamoto, S. Watanabe, Y. Kakinami, T. Yokoyama, J. Klenzing, R. Bishop, R. Walterscheid, M. Yamamoto, Y. Yamazaki
Investigation: R. Pfaff
Methodology: M. Larsen, H. Habu, J. Clemmons, D. Rowland
Supervision: N. Murphy, V. Angelopoulos
Writing - original draft: R. Pfaff

observations on the ground, initially from small deflections of compass needles and later by precise magnetometers. During quiet conditions, these magnetic variations primarily represent currents resulting from upper atmosphere winds driven by solar heating (e.g., Yamazaki & Maute, 2017). This global system of currents at middle and low latitudes comprises the atmospheric daytime dynamo illustrated in Figure 1, in which the external part of the equivalent current calculated from spherical harmonic analysis is shown.

Atmospheric currents are set up by neutral gas motions or winds which, via ion-neutral collisions, drag the ionosphere plasma across the ambient magnetic field, producing a current density, \mathbf{J} , as the ambient ions are collision dominated within the lower ionosphere (90–140 km) yet the electrons are magnetized (Rishbeth & Garriott, 1969). As the winds, \mathbf{U} , push ions across the magnetic field, \mathbf{B} , electromotive fields are set up equivalent to $\mathbf{U} \times \mathbf{B}$. In order to restrict the currents to be nondivergent (i.e., $\nabla \cdot \mathbf{J} = 0$), local polarization electric fields, \mathbf{E} , are created. The total current is thus given by the dynamo equation:

$$\mathbf{J} = \underline{\sigma} \cdot (\mathbf{E} + \mathbf{U} \times \mathbf{B}) \quad (1)$$

where $\underline{\sigma}$ is the conductivity tensor. Despite the fundamental importance of the dynamo current system within the Earth's near-space environment, the factors that contribute to the current in Equation 1 have never been fully measured as a function of altitude, prior to the observations presented here.

The Earth's daytime atmospheric dynamo has generated many decades of research including theory, modeling, and observations that are far too extensive to review here. We nevertheless highlight a few key contributions important for helping to establish the motivation of the experiment discussed in this article. Forbes and Lindzen (1976) and Richmond et al. (1976) showed modeling results that demonstrated that tides were the most likely explanation to establish the dynamo currents and Richmond (1979) established the theoretical electrodynamic framework of the dynamo currents driven by winds. Yamazaki and Maute (2017) provide an extensive review of the current state of research and modeling regarding ionospheric dynamo currents.

Previous rocket experiments designed to study Sq currents were launched near midday at midlatitudes and demonstrated that a distinct layer of currents exist near 105–115 km where the Hall conductivity maximizes. These include rocket measurements from Wallops (Davis et al., 1965), and rocket measurements from Australia (Burrows & Hall, 1965). All of these data were gathered with scalar magnetometers from which a single current direction was derived. Two additional rocket experiments flown from Wallops were reported by Cloutier and Haymes (1968) who used a bias coil linked to the solar aspect angle that varied within the rocket spin to gather vector information from a scalar magnetometer.

Daytime wind measurements using vapor trails, as reported herein, are very scarce, with only two experiments reporting daytime wind observations at midlatitudes in the lower ionosphere, including Hind and Lloyd (1974) from Australia and Rees et al. (1979) from Wallops. Both sets of observations showed moderate- to large-amplitude winds with spiral structure although no association with the dynamo current systems was reported. To our knowledge, there have been no previously reported direct current (DC) electric fields gathered in the daytime dynamo region. Rees and Maynard (1980) reported fields of about 1 mV/m from a rocket launched near 15 LT from Wallops that achieved an apogee of 98.2 km.

One set of previous observations particularly germane to our study involved Arecibo incoherent scatter radar observations of neutral winds and plasma density that were combined with an atmospheric model to compute currents as a function of altitude in the lower ionosphere (Harper, 1977a, 1977b). The height integrated current was then compared with ground-based magnetometer observations of the dynamo current during disturbed conditions. Currents associated with the simultaneously measured *F* region electric field were also computed. Whereas this study did not directly measure currents or DC electric fields in the dynamo region, this research underscores how wind variations might generate currents that vary significantly with altitude in regions of high conductivity and sets the stage for the rocket observations that we present here.

2. Experiment Description

The experiment described herein consisted of a pair of sounding rockets (Figure S1) launched nearly simultaneously from Wallops Island, Virginia (37.83°N, −75.48°E), and flown in conjunction with nearby ground-based magnetometer and ionosonde observations. (The geomagnetic latitude of Wallops is ~50°N.) The first rocket, launched on 4 July 2013 at 14:31:25 UT, attained an apogee of 135 km and

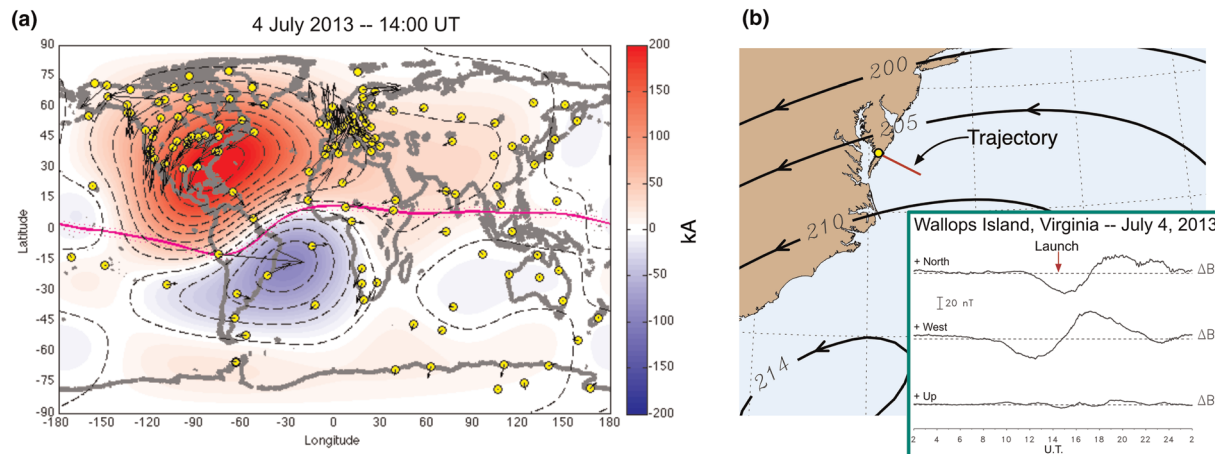


Figure 1. (a) The global dynamo equivalent currents based on worldwide ground magnetometer observations (yellow circles) collected at the time of launch. The pink line represents the magnetic equator. (b) Portion of the dynamo, with contours labeled in kA, showing the Wallops launch range (yellow circle) and the rocket trajectory. The lower panel shows the ground magnetometer data during the launch.

carried direct (also referred to as in situ) instruments. A second rocket was launched 15 s later, reached an apogee of 143 km, and released a vapor trail along its trajectory (Figure S2). A National Aeronautics and Space Administration (NASA) airplane (Figure S3) situated downrange provided views of the trail at 8.2 km altitude from different vantage points (Figure S4).

The rockets were launched during a ΔB_x deflection of -30 nT observed by a ground magnetometer, as shown in Figure 1, indicative of strong westward currents overhead, while a colocated ionosonde observed a normal daytime ionosphere above the range. The geophysical (magnetic) conditions were quiet ($K_p = 1.5$) with slightly positive IMF B_z conditions.

3. Results

We begin with a presentation of the vapor trails that were released from one rocket, followed by a data presentation of the probe measurements gathered from the other, instrumented rocket.

Vapor trails released along rocket trajectories allow the tracking of neutral gas motions (or winds) in the upper atmosphere. For this experiment, lithium vapor was chosen as it produces a bright, narrowband resonant emission at 670.7 nm wavelength in sunlight. The trails covered the altitude range of 90 to 125 km. Clearly visible from cameras with infrared filters in an aircraft at 8.2 km altitude, photographs of the trails are shown in Figure 2. The upper photograph illustrates a smooth wind profile peaking near 108 km altitude while the lower photograph shows turbulent neutral dynamics near 102 km.

The horizontal winds shown in Figure 2 were deduced from the motion of the trail over the period of several minutes in which the trail was observed. The wind peaked at 167 m/s at 108 km and exhibited strong shears with respect to altitude. No vertical motions of the winds were discerned in the visible trails although this is difficult to ascertain from a single observation platform. Accordingly, the displacement of trail features from one image to the next is assumed to be a purely horizontal movement. The uncertainty in the measurement could be as large as ± 12 m/s if the vertical winds were as large as 5 m/s (see supporting information). The wind observations are also consistent with an independent derivation of the wind from ionization gauge sensors on the instrumented rocket (Figure S7).

The Richardson number, defined as the ratio of the Brunt-Vaisala frequency to the square of the wind shear with altitude, is also shown in Figure 2. When this value is less than 0.25, shears are predicted to be unstable (Miles, 1961). Indeed, the lower photograph in Figure 2 reveals turbulent structure corresponding to the largest observed wind shears.

The instrumented rocket was designed to measure the DC electric fields and magnetic fields as well as the gas properties of the lower ionosphere. It included an orthogonal pair of 5 m double probes in the spin

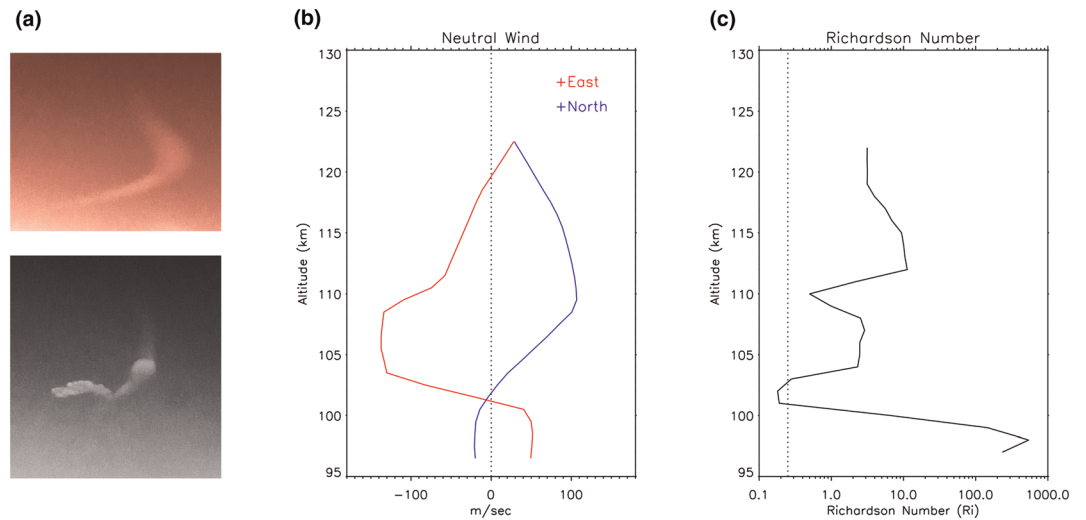


Figure 2. (a) Images of the vapor trail photographed from the NASA aircraft at 8.2 km altitude. The upper image shows the profile near 108 km. The lower image shows turbulence associated with the wind shear near 102 km. (b) Zonal and meridional wind components deduced from the vapor trails. (c) Computed Richardson number based on the observed shears.

plane to measure DC electric fields, a flux-gate vector magnetometer from which currents were derived, a Langmuir probe to measure plasma density, and ionization gauges to measure the neutral density and provide independent information on the winds (Figure S8). An attitude control system oriented the spin axis along the magnetic field direction.

The in situ data from the fields and plasma probes are plotted versus altitude in Figure 3 alongside the winds from the vapor trail. The ion density, measured with a Langmuir probe, shows a typical daytime profile, consistent with the concurrent ground-based ionosonde measurements (Figure S9). Notice the enhanced, narrow layer near 102 km which occurred at the same altitude as the observed neutral wind shear (discussed later).

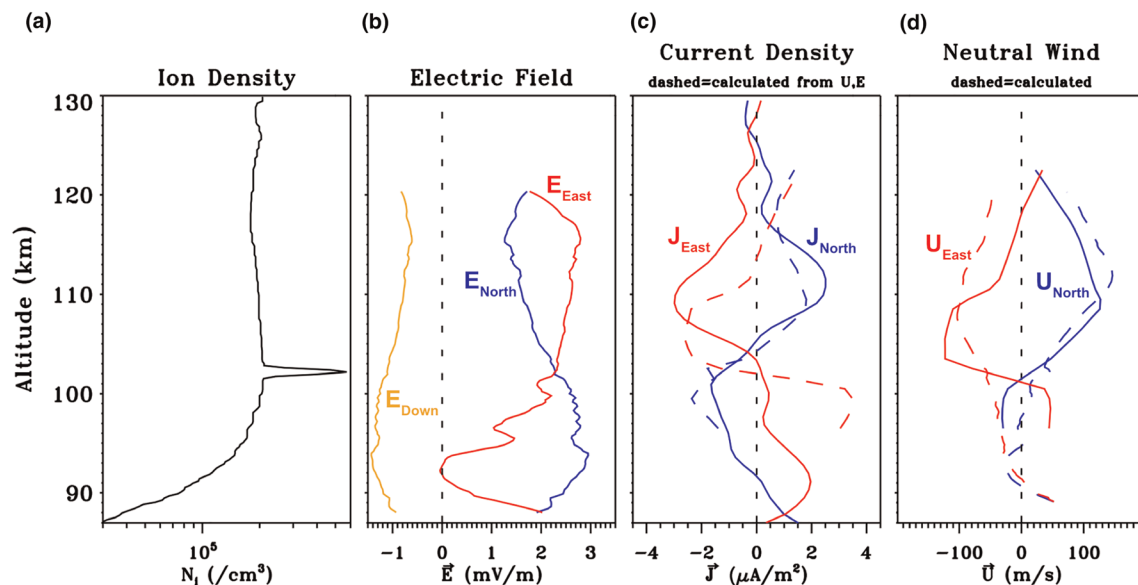


Figure 3. (a) Plasma density from the Langmuir probe. (b) Measured DC electric fields. (c) Current density measurements derived from the magnetic field data. (d) Neutral winds determined from vapor trails photographed from the airplane. (The dashed lines are calculated by solving Equation 1, the dynamo equation.)

The electric field data are shown in the next panel, in which the $\mathbf{V} \times \mathbf{B}$ fields due to the velocity of the rocket, \mathbf{V} , across the ambient magnetic field have been subtracted (Figure S10). In the dynamo region between 100–120 km, the electric field detector measured east-west or zonal components of ~ 2.5 mV/m eastward, corresponding to $\mathbf{E} \times \mathbf{B}$ plasma drifting upward and northward at roughly 50 m/s, and north-south or meridional components of 1–2 mV/m northward, corresponding to westward plasma drifts of 20–40 m/s. The vector data shown here have been converted to “magnetic horizontal” coordinates to facilitate comparisons with the currents and neutral winds. In these coordinates, the two horizontal components have been rotated such that the north component is along the horizontal projection of the magnetic field direction and the east component is along magnetic east. The vertical component remains the same.

Current density profiles in Figure 3c were obtained using $\nabla \times \mathbf{B} = \mu_0 \mathbf{J}$ to convert the observed magnetic field variations (Figures S11 and S12) to currents assuming only variations with altitude measured along the rocket trajectory (μ_0 is the permeability of free space.) In other words, we assume no vertical currents and no variations along the horizontal component of the rocket velocity. Along these lines, we note that the Swarm satellites (Park et al., 2020) show interhemispherical field-aligned currents of several nA/m², which, if these existed in the *E* region, are several orders of magnitude weaker than the horizontal currents we derive here and thus our assumption that they are negligible is valid. The horizontal components thus correspond to $J_{\text{north}} = -dB_{\text{west}}/dz$ and $J_{\text{west}} = dB_{\text{north}}/dz$, where dz corresponds to the variation with respect to altitude. As shown in Figure 3, the measurements reveal westward zonal current densities near $2 \mu\text{A}/\text{m}^2$ peaking near 110 km. Notice the pronounced meridional current of the same magnitude in the northward direction at a slightly higher altitude. Both of these current components changed direction below ~ 103 km.

The plasma density, electric fields, and winds enable the dynamo equation to be evaluated as a function of altitude. In the third panel of Figure 3, the dashed lines show current densities that result from solving the dynamo equation using the measured winds, electric fields, and plasma density. Model atmospheric constituents are used to calculate the collision frequencies in the conductivity tensor (see supplementary material). Similarly, in the fourth panel, the predicted winds based on the measured currents, electric fields, and plasma density are shown by the dashed lines. Notice that above ~ 102 km, there is relatively good agreement between the strongest observed currents and winds with those predicted from the other measurements, supporting the use of the dynamo equation to describe the general electrodynamics. Below 102 km, the weaker observed winds are not well reflected in the predicted currents. This discrepancy requires further evaluation particularly since payload coning effects and increased neutral densities at these lower altitudes can degrade the current and electric field measurement accuracies.

Another important observational result is that the measured currents reveal a spiral pattern consistent with corresponding variations with altitude of the measured winds. This is shown in the wind and current hodograms in Figure 4a and in the three-dimensional representation of the currents and winds versus altitude in Figure 4b. The existence of these interleaved patterns of winds and current densities demonstrates the effectiveness of the winds in setting up local horizontal current sheets and presents a new viewpoint regarding how dynamo currents vary as a function of altitude.

4. Discussion

Comprehensive observations of the Earth’s daytime dynamo have been gathered in conjunction with ground-based instruments. The results provide a new perspective on the nature of upper atmosphere winds, currents, and DC electric fields and their role in forming the worldwide system of dynamo currents as well as our interpretation of ground-based magnetometer observations of quiet ionospheric currents. When analyzed as a whole, the dynamo equation is shown to predict fairly well the currents based on measured wind, electric field, and plasma density profiles. The most significant new results are discussed below, organized according to the neutral winds and shears, current density profiles, and DC electric fields and the dynamo equation.

Upper atmosphere winds and shears. The upper atmospheric daytime winds are considerably larger (>160 m/s) than those predicted by typical solar thermal tides, for example, 20–30 m/s, (e.g., Oberheide et al., 2011). The total wind field also contains a background wind (i.e., a zonal mean wind) of several tens of m/s on which the tidal wind variations, and perhaps those of gravity waves, are superimposed. Nevertheless, the measured

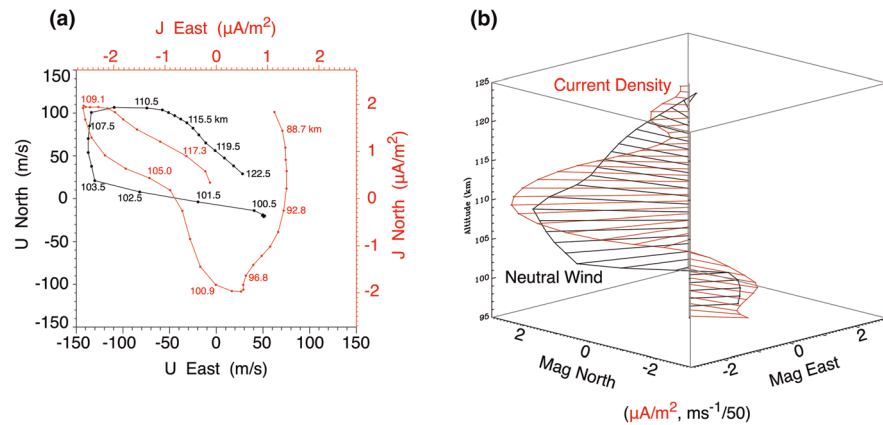


Figure 4. (a) Hodograms showing the horizontal variations of the neutral wind and current density in the zonal and meridional directions. Altitudes are provided along the curves, depicted in kilometers. (b) Three-dimensional representation of the horizontal neutral winds and current density versus altitude showing the interleaved spiral patterns of both measured quantities.

winds are larger than those generally ascribed to tides and to our understanding of mean background winds. On the other hand, the large-amplitude winds measured in this experiment are consistent with a significant data set of large-amplitude, lower ionosphere winds deduced from nighttime vapor trails (Larsen, 2002). The very few previous wind experiments that used vapor trails in the daytime lower thermosphere at midlatitudes also reported large velocities (Hind & Lloyd, 1974; Rees et al., 1979) though not as large as those that we report here.

The winds and currents exhibit an interleaved spiral pattern. That the winds show a rotational pattern (clockwise viewed from above) with increasing amplitudes toward higher altitudes suggest they are tidal in nature and driven from below. The estimated vertical wavelength of the measured winds is roughly 20–30 km, indicative of either diurnal or semidiurnal tides (e.g., J. Forbes, 1995) although such variations may also be due to gravity waves. We note that a similar spiral structure was observed in wind measurements by Hind and Lloyd (1974). Those researchers reported a counter-clockwise rotation that they attributed to the fact their observations were gathered in the southern hemisphere.

The vapor trails show evidence of turbulence where the wind shear is strongest. The Richardson number condition for turbulence is shown to be unstable at 102 km, precisely where large scale neutral structuring and turbulence were observed. The data suggest that such shear-driven neutral turbulence may be very common in the daytime lower ionosphere, coupling in unknown ways with the ambient plasma. Shear instabilities, for example, Kelvin Helmholtz, may also exist, as shown for strong nighttime wind variations in the lower ionosphere (Larsen, 2000).

The altitude of the strongest wind shear is precisely where a distinct sporadic-E layer was observed in the plasma density. That sporadic-E layers are formed by neutral wind shears is well established (e.g., Haldoupis, 2012). The observation of a daytime sporadic-E layer coincident with a strong wind shear helps to promote techniques to infer wind shears and tidal forcing remotely using radiowaves, since sporadic-E layers are observable in radar, ionosonde, and GPS data.

Current density profiles. The observed dominant zonal current was westward, peaking at ~110 km, in agreement with previous rocket measurements using scalar magnetometers at this local time (Burrows & Hall, 1965; Cloutier & Haymes, 1968; Davis et al., 1965) and consistent with the Hall mobility peaking near this altitude at midlatitudes. What is new in the vector magnetometer observations reported here is that the currents reveal a spiral pattern in concert with that of the neutral wind that was not previously recognized. This is clear observational evidence that the dynamo currents are driven by tidal forcing.

The currents inferred from the ground magnetometer data cannot reflect the stratified current amplitudes in the ionosphere. The integrated measured zonal component is generally consistent with the ground ΔB_x measurement of -30 nT, whereas the integrated meridional components cancel, consistent with the small ground ΔB_y measurement. The important result is that the true character of the horizontal currents

cannot be discerned in ground-based data because integrated bidirectional excursions cancel. This is consistent with modeling studies (e.g., Kawano-Sasaki & Miyahara, 2008), which show vertically stratified currents are canceled by height integration.

DC electric fields and the dynamo equation. The measured DC electric fields are consistent with those set up to maintain a divergence-free current system (i.e., $\nabla \cdot \mathbf{J} = 0$) and hence act to balance the currents due to the winds in the dynamo equation. Although the measurements presented here show that both the winds and electric fields were considerably larger than expected, since their current contributions generally counter each other, their critical role in the dynamo process is obscured. In other words, whereas the measured total current densities and ground-based magnetic field deflections appear commensurate with those associated with weak tidal heating, in fact, the forces inherent to the dynamo are much more pronounced, though hidden.

To further appreciate the role of the DC electric fields and the currents associated with it, consider that a poleward (northward) DC electric field drives westward $\mathbf{E} \times \mathbf{B}$ drifts in the region of enhanced Hall mobility in the region of 105–110 km, which correspond to an eastward Hall current. However, the primary zonal current observed in situ and on the ground is clearly westward. This westward current is primarily driven by the strong westward neutral winds. The electric field is set up to drive a current in the opposite direction, thus acting to ensure that the divergence of the currents is zero and, in the process, limiting or “regulating” the zonal current.

The DC electric fields have associated plasma drifts in the same direction, although with somewhat larger amplitudes, than average values at higher altitudes at midlatitudes measured by satellite probes (Heelis & Coley, 1992) and incoherent scatter radars (e.g., Ganguly et al., 1987). How electric fields set up by lower ionosphere winds and currents transfer to higher altitudes via the highly conducting magnetic field is an important topic for future study. The observations presented here nevertheless provide evidence that intrinsic electric fields are generated within the dynamo region and that they subsequently contribute to the Earth's daytime global ionospheric potential at midlatitudes.

Finally, we note that the observed DC electric fields are not constrained with altitude in a similar fashion as that of the winds and currents. Rather, they easily influence neighboring altitudes along the highly conducting magnetic field, which was inclined at $\sim 45^\circ$. This is in contrast to the DC polarization electric fields observed in the equatorial electrojet, which are sustained in the vertical direction within the narrow layer of enhanced Cowling conductivity, (e.g., Pfaff et al., 1997). Accordingly, although the combined measurements reported here show that, as an ensemble, they are generally governed by the dynamo equation (1), these relationships, particularly with respect to the electric fields, are not linear and require a more detailed, nonlocal analysis. Future modeling efforts promise to advance our understanding of the creation and role of DC electric fields in the daytime dynamo process.

5. Summary

For the first time, altitude profiles of the upper atmospheric winds, current density, plasma conductivity, and DC electric fields have been measured simultaneously in the daytime, lower ionosphere. Using this unique measurement set, we are able to solve the dynamo equation as a function of altitude, revealing the contributions of the different sources of energy which drive the lower ionospheric currents. We find that the DC electric fields ($\sim 2\text{--}3$ mV/m) and neutral winds (~ 165 m/s) are of larger than expected magnitudes yet their directions are such that their contributions to the overall dynamo current largely cancel, leaving the net current density to be commensurate with that predicted by weak solar tidal heating of the upper atmosphere. In essence, the forces that set up the dynamo are shown to be larger and more complex than those ascribed to simple tidal interactions.

Furthermore, an important new result is that the vector current density measurements displayed a spiral pattern in concert with the wind profile, providing clear evidence that the Sq currents are driven by tidal forcing. This result underscores that the currents believed responsible for the magnetic variations observed on the ground are not due to a simple overhead current system but, rather, result from complex, stratified current systems that vary considerably with altitude and whose integrated effects produce the observed magnetometer variations on the ground.

Finally, we report that the daytime neutral winds have considerably larger amplitudes than those predicted by simple tidal models, in a similar fashion for nighttime winds in which Larsen (2002) showed those amplitudes to also be greater than those predicted by simple tidal analysis. The existence of strong shears in the observed winds is shown to produce localized neutral turbulence, as predicted by the calculations of the Richardson number, as well as shown directly in the photographs of the observed neutral turbulence reported here. These results underscore that the Earth's upper atmospheric motions are not laminar but include complex structures, shears, and turbulence that couple to the colocated ionospheric plasma in unknown and fascinating ways.

Conflict of Interest

Authors declare no competing interests.

Data Availability Statement

The rocket data supporting this article are publicly available online (<https://rscience.gsfc.nasa.gov/EFITeam/dynamo21140.html>).

Acknowledgments

We thank Steven Martin, NASA/Goddard Space Flight Center, for expert assistance with the data products, calibration, and display, including the ground-based magnetometer data at Wallops. We acknowledge the expertise of the NASA/Wallops Flight Facility in expertly designing, building, testing, and launching the payloads and rocket systems. In this regard, we salute in particular the payload manager, Mr. Jay Scott. U.S. researchers, except N. M. and V. A., were supported by a NASA grant that resulted from a peer-reviewed proposal to NASA's Science Mission Directorate. Contributions from researchers in Japan were supported by the Japanese Aerospace Exploration Agency (JAXA).

References

- Burrows, K., & Hall, S. (1965). Rocket measurements of the geomagnetic field above Woomera, South Australia. *Journal of Geophysical Research*, *70*(9), 2149–2158. <https://doi.org/10.1029/JZ070i009p02149>
- Cloutier, P., & Haymes, R. (1968). Vector measurement of the mid-latitude Sq ionospheric current system. *Journal of Geophysical Research*, *73*(5), 1771–1787. <https://doi.org/10.1029/JA073i005p01771>
- Davis, T., Stolarik, J., & Heppner, J. (1965). Rocket measurements of Sq currents at midlatitude. *Journal of Geophysical Research*, *70*, 5883–5894.
- Forbes, J. (1995). Tidal and planetary waves. In *The upper mesosphere and lower thermosphere* (pp. 67–87). Washington, DC: American Geophysical Union.
- Forbes, J. M., & Lindzen, R. S. (1976). Atmospheric solar tides and their electrodynamic effects—I. The global Sq current system. *Journal of Atmospheric and Terrestrial Physics*, *38*, 897–910.
- Ganguly, S., Behnke, R., & Emery, B. (1987). Average electric field behavior in the ionosphere above Arecibo. *Journal of Geophysical Research*, *92*(A2), 1199–1210. <https://doi.org/10.1029/JA092iA02p01199>
- Haldoupis, C. (2012). Midlatitude sporadic-E. A typical paradigm of atmosphere-ionosphere coupling. *Space Science Reviews*, *168*(1–4), 441–461. <https://doi.org/10.1007/s11214-011-9786-8>
- Harper, R. M. (1977a). A comparison of ionospheric currents, magnetic variations, and electric fields at Arecibo. *Journal of Geophysical Research*, *82*(22), 3233–3242. <https://doi.org/10.1029/JA082i022p03233>
- Harper, R. M. (1977b). Tidal winds in the 100–200 km region at Arecibo. *Journal of Geophysical Research*, *82*(22), 3243–3250. <https://doi.org/10.1029/JA082i022p03243>
- Heelis, R., & Coley, W. (1992). East-west ion drifts at mid-latitudes observed by Dynamics Explorer-2. *Journal of Geophysical Research*, *97*(A12), 19,461–19,469. <https://doi.org/10.1029/92JA01840>
- Hind, A., & Lloyd, K. (1974). A determination of the daytime thermospheric wind profile by observing a lithium trail with a field-of-view scanner. *Australian Journal of Physics*, *41*, 401–410.
- Kawano-Sasaki, K., & Miyahara, S. (2008). A study on three-dimensional structures of the ionospheric dynamo currents induced by the neutral winds simulated by the Kyushu-GCM. *Journal of Atmospheric and Solar - Terrestrial Physics*, *70*(11–12), 1549–1562. <https://doi.org/10.1016/j.jastp.2008.05.004>
- Larsen, M. (2000). A shear instability seeding mechanism for quasiperiodic radar echoes. *Journal of Geophysical Research*, *105*(A11), 24,931–24,940. <https://doi.org/10.1029/1999JA000290>
- Larsen, M. (2002). Winds and shears in the mesosphere and lower thermosphere: Results from four decades of chemical release wind measurements. *Journal of Geophysical Research*, *107*(A8), 1215. <https://doi.org/10.1029/2001JA000218>
- Miles, J. (1961). On the stability of heterogeneous shear flows. *Journal of Fluid Mechanics*, *10*(04), 496–508. <https://doi.org/10.1017/S0022112061000305>
- Oberheide, J., Forbes, J., Zhang, X., & Bruinsma, S. (2011). Climatology of upward propagating diurnal and semidiurnal tides in the thermosphere. *Journal of Geophysical Research*, *116*, A11306. <https://doi.org/10.1029/2011JA016784>
- Park, J., Yamazaki, Y., & Lühr, H. (2020). Latitude dependence of Interhemispheric Field-Aligned Currents (IHFACs) as observed by the Swarm constellation. *Journal of Geophysical Research: Space Physics*, *125*, e2019JA027694. <https://doi.org/10.1029/2019JA027694>
- Pfaff, R., Acuna, M., Mariotti, P., & Trivedi, N. (1997). DC polarization electric field, current density, and plasma density measurements in the daytime equatorial electrojet. *Geophysical Research Letters*, *24*(13), 1667–1670. <https://doi.org/10.1029/97GL01536>
- Rees, D., & Maynard, N. (1980). Midlatitude measurements of the ionospheric electric field during the ALADDIN programme. *Journal of Atmospheric and Terrestrial Physics*, *42*(6), 577–582. [https://doi.org/10.1016/0021-9169\(80\)90068-9](https://doi.org/10.1016/0021-9169(80)90068-9)
- Rees, D., Rounce, P., Best, G., & Quesda, A. (1979). Midlatitude measurements of the thermospheric neutral wind during the ALADDIN programme. *Journal of Atmospheric and Solar - Terrestrial Physics*, *41*, 1117–1178.
- Richmond, A. D. (1979). Ionospheric wind dynamo theory: A review. *Journal of Geomagnetism and Geoelectricity*, *31*(3), 287–310. <https://doi.org/10.5636/jgg.31.287>
- Richmond, A. D., Matsushita, S., & Tarpley, J. D. (1976). On the production mechanism of electric currents and fields in the ionosphere. *Journal of Geophysical Research*, *81*(4), 547–555. <https://doi.org/10.1029/JA081i004p00547>
- Rishbeth, H., & Garriott, O. (1969). *Introduction to ionospheric physics*, *International Geophysics Series*, New York: Academic Press.

Yamazaki, Y., & Maute, A. (2017). Sq and EEJ—A review on the daily variation of the geomagnetic field caused by ionospheric dynamo currents. *Space Science Reviews*, 206(1-4), 299–405. <https://doi.org/10.1007/s11214-016-0282-z>

References From the Supporting Information

- Banks, P., & Kockarts, G. (1973). *Aeronomy, Part B*. New York: Academic Press.
- Bedinger, J. (1973). Photography of a lithium vapor trail during the daytime. *Journal of Atmospheric and Solar - Terrestrial Physics*, 35(2), 377–381. [https://doi.org/10.1016/0021-9169\(73\)90105-0](https://doi.org/10.1016/0021-9169(73)90105-0)
- Best, G. (1974). New high altitude vapor trail tracking techniques. *Journal of Atmospheric and Solar - Terrestrial Physics*, 36(3), 501–511. [https://doi.org/10.1016/0021-9169\(74\)90129-9](https://doi.org/10.1016/0021-9169(74)90129-9)
- Bilitza, D., McKinnell, L.-A., Reinisch, B., & Fuller-Rowell, T. (2011). The international reference ionosphere today and in the future. *Journal of Geodesy*, 85(12), 909–920. <https://doi.org/10.1007/s00190-010-0427-x>
- Brace, L. (1998). Langmuir probe measurements in the ionosphere. In *Measurement techniques in space plasmas: Particles* (pp. 23–35). Washington, DC: American Geophysical Union.
- Butko, A. (1974). Wind measurements using magnetometer, optical, and static pressure sensors. *Advances in Space Research*, 14, 117–118.
- Horowitz, R., & LaGow, H. (1957). Upper air pressure and density measurements from 90 to 220 kilometers with the Viking 7 rocket. *Journal of Geophysical Research*, 62(1), 57–78. <https://doi.org/10.1029/JZ062i001p00057>
- Maynard, N. C. (1998). Electric field measurements in moderate to high density space plasmas with passive double probes. In *Measurement techniques in space plasmas: Fields* (pp. 13–27). Washington, DC: American Geophysical Union.
- Picone, J., Hedin, A., Drob, D., & Aikin, A. (2002). NRLMSISE-00 empirical model of the atmosphere: Statistical comparisons and scientific issues. *Journal of Geophysical Research*, 107(A12), 1468. <https://doi.org/10.1029/2002JA009430>
- Thébault, E., Finlay, C., Beggan, C., Alken, P., Aubert, J., Barrois, O., et al. (2015). International geomagnetic reference field: The 12th generation. *Earth, Planets and Space*, 67(1), 79. <https://doi.org/10.1186/s40623-015-0228-9>